# Insight into the local environment of magnesium and calcium in low-coordination number organocomplexes using $^{25}$Mg and $^{43}$Ca solid state NMR: a DFT study

**Christel Gervais,[a,*] Cameron Jones,[b] Christian Bonhomme,[a] Danielle Laurencin[c,*]**

[a]Sorbonne Universités, UPMC Univ Paris 06, Collège de France, UMR CNRS 7574, Laboratoire de Chimie de la Matière Condensée de Paris, 4 place Jussieu, 75252 Paris cedex 05, France; [b] School of Chemistry, Monash University, PO Box 23, Victoria 3800, Australia; [c]Institut Charles Gerhardt de Montpellier, UMR5253, CNRS UM ENSCM, CC1701, Pl. E. Bataillon, 34095 Montpellier cedex 05, France. Correspondence emails : christel.gervais_stary@upmc.fr, danielle.laurencin@umontpellier.fr

**Synopsis** DFT calculations of $^{25}$Mg and $^{43}$Ca NMR parameters were performed on crystal structures of organomagnesium and organocalcium complexes involving low-coordination numbers and N-bearing ligands. It is shown how these spectroscopies may be used for these systems for NMR crystallography approaches.

**Abstract** With the increasing number of organocalcium and organomagnesium complexes under development, there is a real need to be able to characterize in detail their local environment in order to fully rationalize their reactivity. For crystalline structures, in cases when the diffraction techniques are insufficient, additional local spectroscopies like $^{25}$Mg and $^{43}$Ca solid state NMR may provide valuable information to help fully establish the local environment of the metal ions. In this manuscript, a prospective DFT investigation on crystalline magnesium and calcium complexes involving low-coordination numbers and N-bearing organic ligands was carried out, in which the $^{25}$Mg and $^{43}$Ca NMR parameters (isotropic chemical shift, chemical shift anisotropy (CSA), and quadrupolar parameters) were calculated for each structure. The analysis of the calculated parameters in relation with the local environment of the metals ions revealed that they are highly sensitive to very small changes in geometry / distances, and hence that they could be used to assist in the refinement of crystal structures. Moreover, such calculations provide a guideline as to how the NMR measurements will need to be performed, revealing that these will be very challenging.

**Keywords: NMR, $^{25}$Mg, $^{43}$Ca, organocomplexes, GIPAW.**

## 1. Introduction

Calcium and magnesium are the two most abundant alkaline earth metals. They are widespread in nature, being among the 10 most abundant elements in the Earth's crust and among the 12 most abundant elements in the human body. They belong to the so-called family of "rock-forming elements", and are present in natural minerals in association with carbonates (e.g. calcite, magnesite, dolomite), phosphates (e.g. francolite, struvite), silicates (e.g. akermanite), sulfates (e.g. gypsum, epsomite), and chlorides (e.g. carnallite, antarcticite)… In the body, they can be found in the mineral phase of bones and teeth, in the active sites of enzymes (e.g. calmodulin), and in the physiological fluids, and they play a key role in signal transduction.

In addition to their high abundance, their low toxicity and light weight makes them interesting elements for the fabrication of functional materials. For example, cement and plaster are two key construction materials which contain calcium, while Mg-based alloys are essential parts of modern vehicles. Mg-based electrodes for Mg- batteries and calcium-pyrophosphate based bioglasses are other examples of the many advanced functional materials currently under study in research laboratories (Murgia *et al.,* 2015; Soulié *et al.*, 2016).

In the field of molecular chemistry, organomagnesium and organocalcium complexes are of great interest for organic synthesis. While Grignard reagents have been known and used for over 100 years, an increasing number of purposely designed Mg and Ca complexes find applications in catalysis. Within these complexes, the Lewis acidity of the metal cation and the nucleophilicity of the organic ligands both play an important role in chemical conversion (Harder *et al.*, 2013; Torvisco *et al.*, 2011; Kobayashi *et al.*, 2011; Sarrazin *et al.*, 2016). The reactivity of the metal ion strongly depends on its local environment and oxidation state, and hence it is important to determine them precisely. While X-ray diffraction is commonly used to characterize the metal ion environments in crystalline forms of these molecules, to the best of our knowledge, $^{43}$Ca and $^{25}$Mg solid state NMR have not been used yet.

$^{25}$Mg and $^{43}$Ca are both difficult nuclei to study by NMR (Freitas *et al.*, 2012; Laurencin *et al.*, 2013; Schurko *et al.*, 2015). Indeed, magnesium-25 is a quadrupolar nucleus (I = 5/2) with a moderate quadrupole moment (Q = 199.4 mbarn), a low natural abundance (10%) and a very low Larmor frequency ($\nu_0$ = 52.0 MHz at $B_0$ = 20 T), while calcium-43 is a quadrupolar nucleus (I = 7/2) with a small quadrupole moment (Q = −44.4 mbarn), a very low natural abundance (0.14%) and also a very low Larmor frequency ($\nu_0$ = 57.2 MHz at $B_0$ = 20 T). Despite these "unfavourable" nuclear spin properties, the development of (ultra-)high magnetic field magnets and of pulse sequences specific to quadrupolar nuclei has resulted in $^{25}$Mg and $^{43}$Ca NMR becoming more accessible (Perras *et al.*, 2013; Schurko, 2013)**,** and it has been shown that these spectroscopies can be very informative on the local structure around calcium and magnesium in a variety of materials (Cahill *et al.*, 2009; Pallister *et al.*,

2009; Freitas *et al.*, 2012; Laurencin *et al.*, 2013), including crystalline molecular complexes (Sene *et al.*, 2013; Sene *et al.*, 2015; Burgess *et al.*, 2013; Burgess *et al.*, 2014). In a number of cases, computational methods involving density-functional theory (DFT) calculations of NMR parameters have also been used to assist in the interpretation of the NMR spectra (Bonhomme *et al.*, 2012a), because the calculation of $^{25}$Mg and $^{43}$Ca NMR parameters can be performed with high accuracy (Laurencin *et al.*, 2012; Gervais *et al.*, 2008). Moreover, such computational methods can also serve as a guideline to determine the acquisition conditions that need to be used for recording the NMR spectra, which can be particularly useful when starting studies on new families of compounds. Indeed, the calculated quadrupolar parameter $C_Q$ can help determine at what field and under what conditions (static or magic angle spinning) the measurements need to be performed.

In this article, we report DFT calculations of the $^{25}$Mg and $^{43}$Ca NMR parameters for a series of crystal structures involving organomagnesium and organocalcium complexes, in which the alkaline earth metal ions have low coordination numbers and are mainly coordinated to N-bearing ligands. The compounds studied were selected as representative examples of the types of systems currently developed in molecular chemistry (Torvisco *et al.*, 2011). The values of the calculated NMR parameters are discussed in view of the local environment of the magnesium and calcium, and it is shown in what way they can be used for "NMR crystallography" types of applications (Harris *et al*., 2009), to help refine crystal structures. Moreover, acquisition conditions for recording the spectra of such complexes are also proposed, opening the way to future experiments on these systems.

## 2. Computational details

DFT calculations were performed on a total of 20 different structures. These were selected on the basis of *(i)* the quality of the X-ray diffraction data, *(ii)* the size of the unit cell, *(iii)* the presence of hydrogen atoms in the published structures (these H positions having been either determined from the F-maps and refined with isotropic thermal parameters, or placed geometrically and refined using a riding model). The reference CCDC .cif file numbers of the structures which were studied are the following (together with the experimental temperatures at which the XRD measurements were performed): 255198 (T = 213 K), 704097 (T = 150 K), 255195 (T = 100 K), 255196 (T = 100 K), 198356 (T = 90 K), 247152 (T = 96 K) and 244505 (T = 173 K) for Ca, and 198354 (T = 96 K), 1207191 (T = 130 K), 266469 (T = 100 K), 1477718 (T = 123 K), 175074 (T = 123 K), 266470 (T = 100 K), 266468 (T = 100 K), 745088 (T = 123 K), 661565 (T = 123 K), 247151 (T = 95 K), 266465 (T = 100 K), 266466 (T = 100 K), 266464 (T = 100 K) for Mg. For each structure, calculations of NMR parameters were performed after geometry optimization of either the H positions or all atom positions. The cell parameters were kept fixed to the experimental values during the optimization. In the case of the structure CCDC 198354 (in which the highest quadrupolar coupling constants were found), no strong

changes in calculated NMR parameters were observed when optimizing the cell parameters (see Supporting information, Table S1).

NMR chemical shift calculations were performed within the DFT formalism using the QUANTUM ESPRESSO (QE) software (Giannozzi *et al.*, 2009). The PBE generalized gradient approximation (Perdew *et al.*, 1996) was used and the valence electrons were described by norm conserving pseudopotentials (Troullier *et al.*, 1991) in the Kleinman Bylander form (Kleinman *et al.*, 1982). The Mg pseudopotential was generated by D. Ceresoli and exported from his web site (Ceresoli, 2016). The Ca pseudopotential used here is the same as in some of our previous work (Gras *et al.*, 2016). Spin-orbit relativistic effects were neglected in the present account; their inclusion in the DFT calculations would possibly lead to small changes for light-weight elements like Ca and Mg (Komorovsky *et al.*, 2015). Dispersion corrections were not included, as they were found to have no strong effect on the calculated NMR parameters for the systems studied here (see Table S2). Because of the large cell sizes, the Γ point was used for the Brillouin zone integration in most calculations to reduce computational cost, because no strong variation in the calculated NMR parameters was found for higher k-point meshes (see supporting information Tables S1 and S3; for structures 198654 and 247152). A plane wave energy cut-off of 80 Ry was used for Ca-based systems, and 60 or 80 Ry for Mg systems. Comparisons of calculations with cut-off values of 60 and 80 Ry on the Mg structure 198354 are shown in the supporting information (Table S1).

The shielding tensor was computed using the Gauge Including Projector Augmented Wave (GIPAW) approach (Pickard *et al.*, 2001), which enables the reproduction of the results of a fully converged all electron calculation (Lejaeghere *et al.,* 2016). Absolute shielding tensors were obtained. To set the $^{43}$Ca chemical shift scale, as previously described (Gervais *et al.*, 2008), the calculated $\delta_{iso}$ for a series of reference compounds were compared to experimental values so that the average sum of experimental and calculated shifts coincide (equations can be found in supporting information, Table S4 and Figure S1). The same procedure was applied for the $^{25}$Mg chemical shift scale, and the comparison between calculated and experimental data is presented in supporting information (Table S5 and Figure S2); the slope of the linear correlation was fitted freely to allow extraction of $\sigma_{ref}$.

Diagonalization of the symmetric part of the calculated tensor then provides its principal components $\sigma_{11}$, $\sigma_{22}$, $\sigma_{33}$ from which the chemical shift components $\delta_{11}$, $\delta_{22}$, $\delta_{33}$ can be calculated. $\delta_{11}$, $\delta_{22}$ and $\delta_{33}$ are defined such as $|\delta_{33} - \delta_{iso}| \geq |\delta_{11} - \delta_{iso}| \geq |\delta_{22} - \delta_{iso}|$, and $\delta_{iso} = 1/3(\delta_{11} + \delta_{22} + \delta_{33})$. The chemical shift anisotropy (CSA) parameters are defined by $\Delta_{CSA} = \delta_{33} - \delta_{iso}$ and $\eta_{CSA} = |(\delta_{22} - \delta_{11})/\Delta_{CSA}|$ (Haeberlen convention) (Haeberlen, 1976). The principal components $V_{xx}$, $V_{yy}$, and $V_{zz}$ of the electric field gradient (EFG) tensor (defined as $|V_{zz}| \geq |V_{xx}| \geq |V_{yy}|$) are obtained by diagonalization of the traceless EFG tensor. The quadrupolar interaction can then be characterized by the quadrupolar coupling constant $C_Q$ and the asymmetry parameter $\eta_Q$, which are defined as: $C_Q = eQV_{zz}/h$ and $\eta_Q = (V_{yy}-V_{xx})/V_{zz}$ (e is the proton charge, h Planck's constant and Q the quadrupole moment of the considered nucleus). The experimental

values of the quadrupole moment of $^{25}$Mg (Q = 19.94 × $10^{-30}$ $m^2$) and $^{43}$Ca (Q = –4.44 × $10^{-30}$ $m^2$) were used to calculate $C_Q$ (Pyykkö 2008; Burgess *et al,* 2014). All calculated values are at 0 K.

Simulations of spectra were performed using the DMFit (Massiot *et al.*, 2002) and QUEST (Perras *et al.*, 2012) programs. The Euler angles reported describe the relative orientation of the EFG tensor with respect to the shielding tensor; they are provided in the relevant Tables in Supporting Information.

## 3. Results and discussion

### 3.1. Calcium complexes

The coordination environments around calcium in six of the complexes studied here are shown in Figure 1. The cation is linked to 3- to 4-ligands, two of which correspond to bulky silylated amines. For the 3-coordinate systems (Figures 1a-b), a nearly planar arrangement of the atoms around the metal cation is observed, the X-Ca-X' angles ranging between ~105 and 135°. In the 4-coordinate systems (Figures 1c-f), the ligands are positioned in a tetrahedral configuration around the metal, but these tetrahedra are distorted, as shown by the unequal Ca…X distances (see supporting information, Tables S6 to S11), and the range of X-Ca-X' angles (between ~80° and 140° depending on the complex). These environments are very different from the 5 to 8- coordination spheres of most Ca(II) compounds (Sowrey *et al.*, 2004; Wong *et al.*, 2008; Burgess *et al.*, 2014; Gambuzzi *et al.*, 2015). The calculated $^{43}$Ca NMR parameters for the 3-coordinate structures are reported in Table 1, and those of the 4-coordinate structures in Table 2.

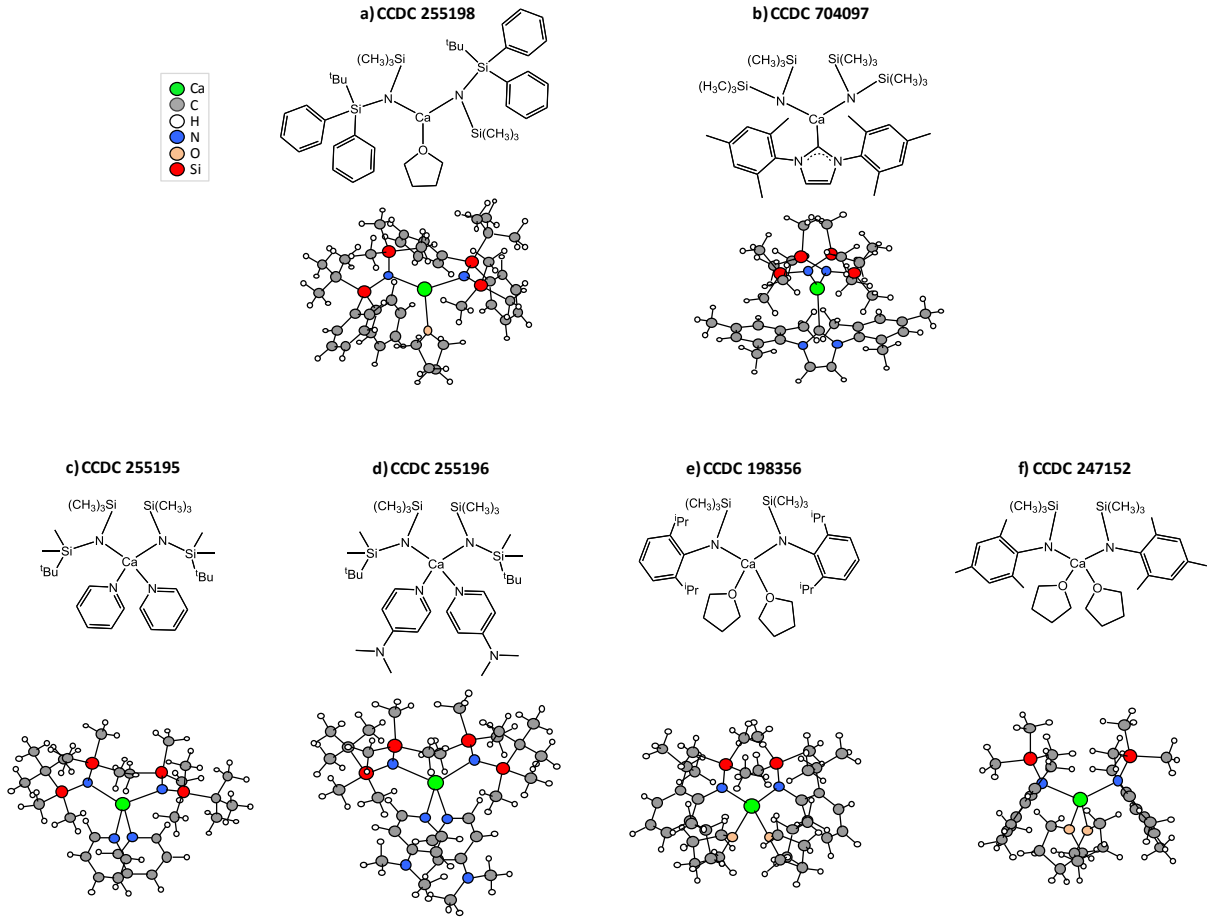


**Figure 1** Representation of the calcium local environment in the complexes studied by DFT. The CCDC references of the corresponding crystal structures are: a) 255198 (Tang *et al.*, 2005a), b) 704097 (Barrett *et al.*, 2008), c) 255195 (Tang *et al.*, 2005a), d) 255196 (Tang *et al.*, 2005a), e) 198356 (Vargas *et al.*, 2002), f) 247152 (Gillett-Kunnath *et al.*, 2005).

**Table 1** DFT-calculated $^{43}$Ca NMR parameters for the 3-coordinate Ca-organocomplexes shown in Figure 1.

| **CCDC** | **255198** | **704097** |
|---|---|---|
| $\delta_{iso}$ (ppm) | 99.5 *(94.8)* | 135.4 *(133.4)* |
| $C_Q$ (MHz) | 8.01 *(7.81)* | −9.92 *(−9.88)* |
| $\eta_Q$ | 0.82 *(0.77)* | 0.41 *(0.45)* |
| $\Delta_{CSA}$ (ppm) | −156.8 *(−155.4)* | 189.6 *(187.2)* |
| $\eta_{CSA}$ | 0.66 *(0.63)* | 0.27 *(0.32)* |
| d(Ca…X) (Å) | 2.34 *(2.37)* | 2.39 *(2.40)* |

Values in parentheses (in italic) were obtained after geometry optimization of all atomic positions, while all other values correspond to H-atom optimization only. d(Ca…X) corresponds to the average Ca…X distance (X = N, O or $C_{NHC}$, where NHC refers to the N-heterocyclic carbene ligand). The equation used to derive calculated shifts from calculated shieldings can be found in supporting information (Figure S1).)

**Table 2** DFT-calculated $^{43}$Ca NMR parameters for the 4-coordinate Ca-organocomplexes shown in Figure 1.

| **CCDC** | **255195** | **255196** | **198356** | | **247152** |
|---|---|---|---|---|---|
| Site | Ca(1) | Ca(1) | Ca(1) | Ca(2) | Ca(1) |
| $\delta_{iso}$ (ppm) | 103.3 *(101.3)* | 106.0 *(99.4)* | 96.3 *(82.9)* | 94.2 *(81.1)* | 102.1 *(89.6)* |
| $C_Q$ (MHz) | −6.11 *(−6.02)* | −6.68 *(−6.32)* | 5.08 *(5.25)* | 5.17 *(5.35)* | 7.22 *(6.28)* |
| $\eta_Q$ | 0.85 *(0.86)* | 0.61 *(0.72)* | 0.87 *(0.84)* | 0.97 *(0.93)* | 0.15 *(0.41)* |
| $\Delta_{CSA}$ (ppm) | 121.7 *(122.8)* | 113.4 *(109.2)* | −99.8 *(−102.5)* | −95.7 *(−99.7)* | −141.6 *(−128.6)* |
| $\eta_{CSA}$ | 0.95 *(0.94)* | 0.88 *(0.97)* | 0.81 *(0.81)* | 0.82 *(0.81)* | 0.17 *(0.28)* |
| d(Ca…X) (Å) | 2.44 *(2.45)* | 2.43 *(2.46)* | 2.34 *(2.38)* | 2.34 *(2.38)* | 2.32 *(2.36)* |

Values in parentheses in italic were obtained after geometry optimization of all atomic positions, while all other values correspond to H-atom optimization only. d(Ca…X) corresponds to the average Ca…X distance (X = N, O). The equation used to derive calculated shifts from calculated shieldings can be found in supporting information (Figure S1).)

Overall, the calculated isotropic chemical shifts ($\delta_{iso}$ > 80 ppm), quadrupolar coupling constants ($|C_Q|$ > 5 MHz) and CSA spans ($|\Delta_{CSA}|$ > 90 ppm) were found to be larger than those reported in previous experimental $^{43}$Ca NMR studies on organic and inorganic materials, in which the metal is mainly surrounded by O-bearing ligands and has higher coordination numbers (Laurencin *et al.*, 2013; Burgess *et al.*, 2014; Widdifield *et al.*, 2014). The high isotropic chemical shifts can be explained by the short average Ca…X distances (Laurencin *et al.*, 2013), while the large $C_Q$ values are due to the anisotropy of the electron distribution around the calcium, which depends on the way in which the 3 (or 4) ligands are positioned around the metal. For the complexes presented in Figure 1, smaller quadrupolar parameters were found for the 4-coordinate systems than the 3-coordinate ones, in agreement with the more symmetric electron distribution in the former case. Interestingly, the calculated CSA span $|\Delta_{CSA}|$ was found to globally increase as a function of $|C_Q|$ (Figure 2a), and the CSA and EFG sensors appeared to have similar directions (Principal Axes Sytems, PAS) for several compounds (Figures 2b-d). In the case of the 3-coordinate complex involving an N-heterocyclic carbene ligand (Figure 1b), the eigenvectors corresponding to $\delta_{22}$ and $V_{yy}$ eigenvalues were actually along the Ca-$C_{NHC}$ direction (Figure 2c).

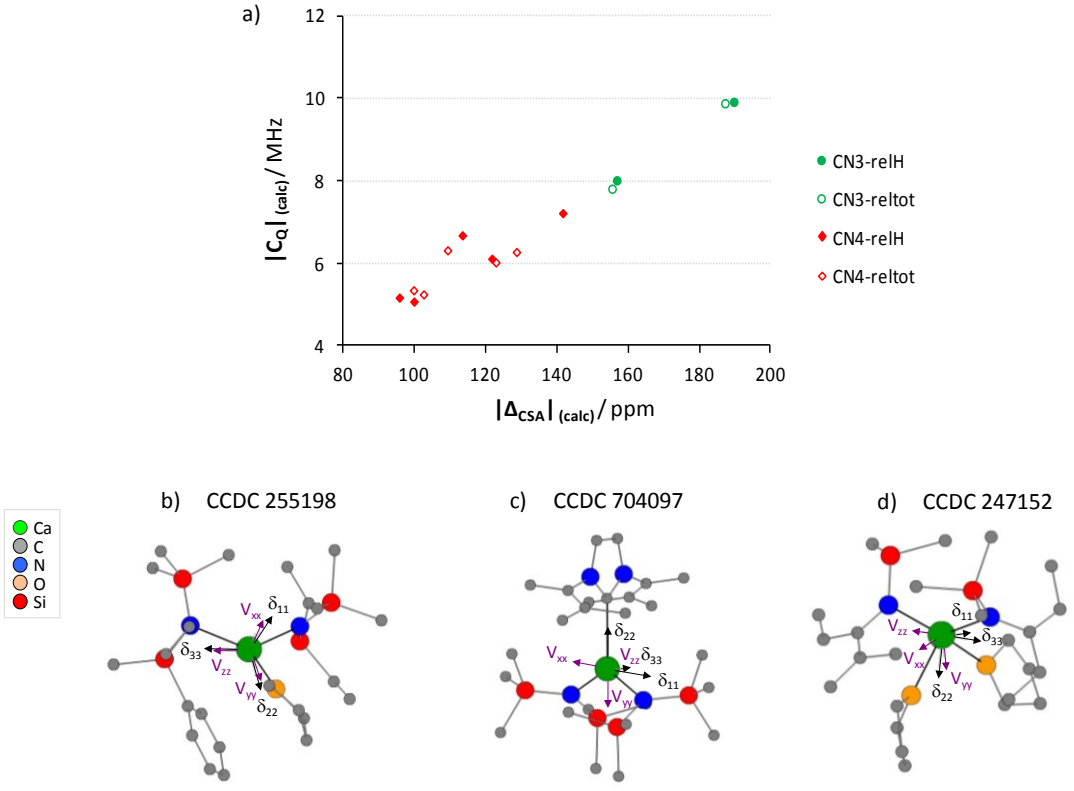


**Figure 2** a) Correlation between $|\Delta_{CSA}|$ and $|C_Q|$ for the organocomplexes shown in Figure 1, depending on the coordination number (CN) of the Ca (CN = 3 in green, CN = 4 in red); b-d) Relative orientations of the shielding and EFG tensors in structures CCDC 255198, 704097 and 247152 (for clarity, only the non-H atoms within a 5 Å radius around the Ca are shown here; Euler angles can be found in Supporting Information – Table S12).

The calculated values provide important guidelines for determining how to record $^{43}$Ca NMR spectra for such compounds. For measurements under MAS (Magic Angle Spinning) conditions, from which $\delta_{iso}$ and the quadrupolar parameters can be extracted, ultra-high magnetic fields ($B_0 \geq 20$ T) with rotors spinning at 10 kHz (*at least*) should to be used, in order to avoid any overlap between the central transition and the associated spinning sidebands (see supporting information, Figure S3). Measurements under static conditions may also be interesting to carry out at high field, in order to extract the CSA parameters (Figure S4). The $^{1}$H…$^{43}$Ca dipolar couplings being very weak (~400 Hz to the most), $^{1}$H decoupling is not expected to significantly improve the measurement under MAS conditions, while it will be needed for static measurements. Due to the very low natural abundance of calcium-43, isotopic enrichment will most probably be necessary for both static and MAS experiments (Laurencin *et al.*, 2013), which implies that the synthetic procedures of these compounds will need to be adapted, because the commercially available $^{43}$Ca-enriched precursor is *$CaCO_3$.

The comparison of calculated $^{43}$Ca parameters after H-atom optimization and full geometry optimization is also worth discussing. Indeed, it shows the very strong sensitivity of $\delta_{iso}(^{43}Ca)$ to the average Ca…X distance, which depends on the nature of the atoms directly linked to the Ca and the bulkiness of the ligands involved. For changes of more than 0.03 Å in this average distance, the calculated $\delta_{iso}(^{43}Ca)$ varies by more than 5 ppm (see Tables 1 and 2). In contrast, for the two structures for which there are the least variations in the local geometry around calcium (CCDC 704097 and 255195 – see Tables S7 and S8), $\delta_{iso}(^{43}Ca)$ varies by less than 2 ppm. Overall, this shows that $^{43}$Ca NMR experiments, in combination with DFT calculations, can be used to contribute to the determination of crystal structures in cases when no single crystal data is available, and/or to their refinement. A typical system for which this would be useful is that of a diketiminato complex described by Avent and co-workers (Figure S5, supporting information), for which the crystal structure published shows disorder in some of the carbon positions (Avent *et al.*, 2005). DFT calculations were performed on a model of this structure (after proposing atomic positions for the partially occupied crystallographic sites). A comparison of the NMR parameters derived from H-relaxation and full relaxation is reported in the supporting information (Table S13). The value of $\delta_{iso}(^{43}Ca)$ changes by nearly 15 ppm between H-relaxed and fully relaxed structures, as a reflection of the significant modifications in the Ca local environment upon full geometry optimization (Table S14). Recording the experimental $^{43}$Ca NMR spectrum for this compound, and comparing experimental and calculated $^{43}$Ca NMR parameters would therefore be useful in trying to refine better this structure.

### 3.2. Magnesium complexes

The local environments around Mg in the 12 complexes which we studied here are shown in Figure 3. In most cases, the oxidation state of Mg is +II, except for compounds CCDC 1477718 (Figure 3d), 745088 (Figure 3h) and 661565 (Figure 3i), which correspond to diamagnetic Mg(I) dimers. The ligands which are coordinated to the metal cation through N- atoms are bulky silylated amines, guanidinates, diketiminates and pyridine (or its derivative), while the O-bearing ligands are ethers (diethylether and tetrahydrofuran). The coordination numbers for these compounds range from 2 to 4, which is low compared to what is most often observed for Mg complexes (Freitas *et al.*, 2009). For each complex, the distances between the Mg and its nearest neighbors are reported in Tables S15-S26. In the 2-coordinate Mg(II) complexes, the N-Mg-N angles vary from ~140° (structure 266469), to ~160° (structure 1207191) and 180° (structure 198354). Concerning the 3-coordinate Mg(II) systems, the coordinating atoms are almost in the same plane as the Mg, and the X-Mg-X' angles vary from ~90 to ~145°. The 4-coordinate complexes display a tetrahedral arrangement of the coordinating atoms around the magnesium, although, just like in the case of calcium, the tetrahedra are distorted due to distributions in the Mg…X distances (see Tables S24 to S26) and the X-Mg-X' angles (from ~95 to ~135°). The calculated $^{25}$Mg NMR parameters for each of these structures are reported in Tables 3 to 5.

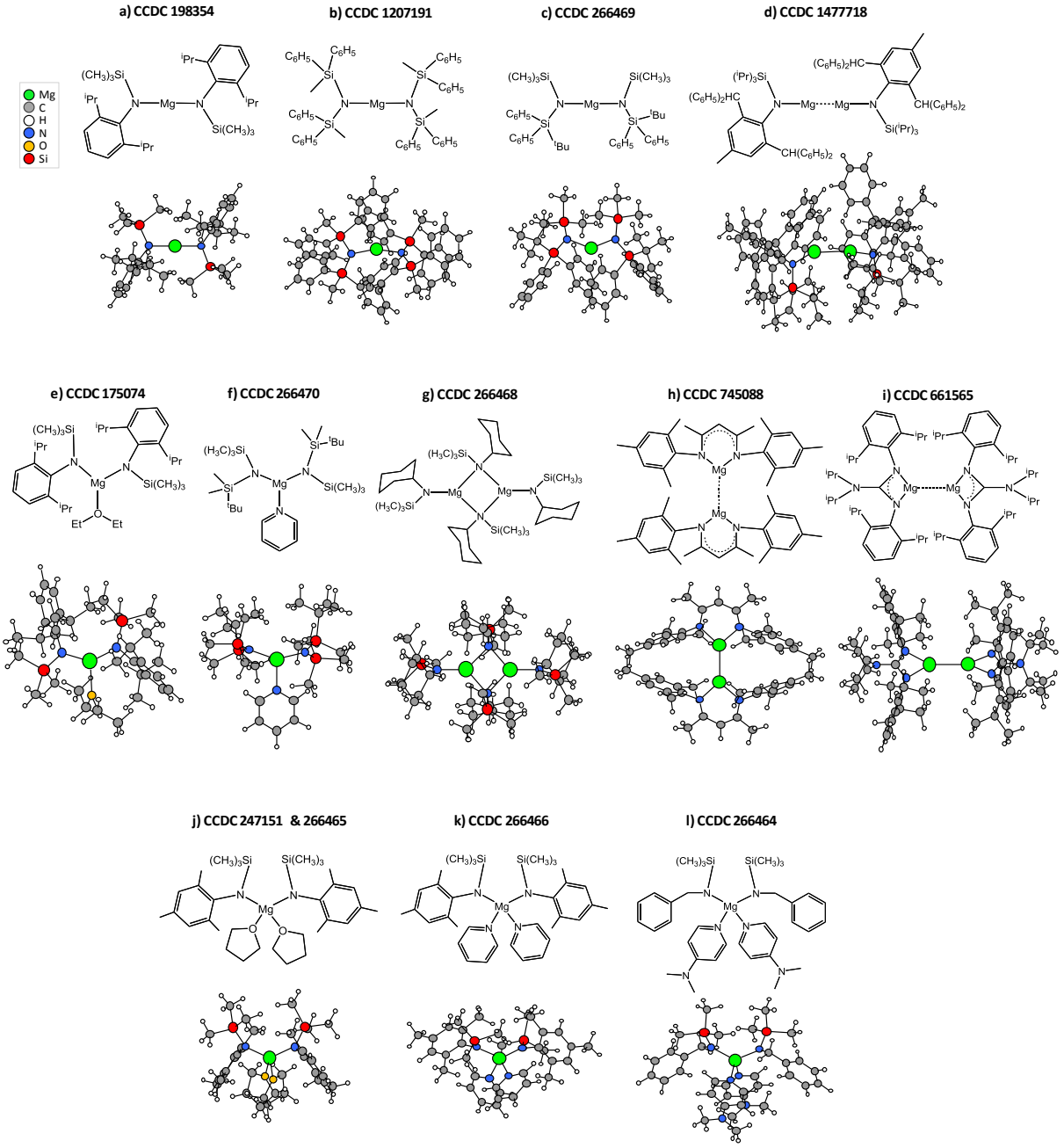


**Figure 3** Representation of the magnesium local environment in the complexes studied here by DFT. The CCDC references of these complexes are: a) 198354 (Vargas *et al.*, 2002), b) 1207191 (Bartlett *et al.*, 1994), c) 266469 (Tang *et al.*, 2005b), d) 1477718 (Boutland *et al.*, 2016), e) 175074 (Kennedy *et al.*, 2001), f) 266470 (Tang *et al.*, 2005b), g) 266468 (Tang *et al.*, 2005b), h) 745088 (Bonyhady *et al.*, 2010), i) 661565 (Green *et al.*, 2007), j) 247151/266465 (Gillett-Kunnath *et al.*, 2005; Tang *et al.*, 2005b), k) 266466 (Tang *et al.*, 2005b) and l) 266464 (Tang *et al.*, 2005b).

**Table 3** DFT-calculated $^{25}$Mg NMR parameters for the "2-coordinate" Mg-organocomplexes shown in Figure 3.

| **CCDC** | **198354** | | **1207191** | **266469** | **1477718** | |
|---|---|---|---|---|---|---|
| Site | Mg(1) | Mg(2) | Mg(1) | Mg(1) | Mg(1) | Mg(2) |
| $\delta_{iso}$ (ppm) | 46.3 *(43.3)* | 49.0 *(45.5)* | 41.6 *(40.7)* | 40.0 *(37.7)* | 53.5 *(50.0)* | 62.1 *(59.1)* |
| $C_Q$ (MHz) | −44.80 *(−43.36)* | −45.69 *(−44.15)* | −36.68 *(−35.94)* | −29.78 *(−29.26)* | −30.97 *(−30.02)* | −32.01 *(−31.27)* |
| $\eta_Q$ | 0.23 *(0.24)* | 0.23 *(0.23)* | 0.06 *(0.06)* | 0.16 *(0.14)* | 0.20 *(0.22)* | 0.11 *(0.11)* |
| $\Delta_{CSA}$ (ppm) | −144.4 *(−140.6)* | −143.7 *(−139.4)* | −120.8 *(−119.5)* | −89.3 *(−90.6)* | −148.1 *(−142.5)* | −158.5 *(−154.2)* |
| $\eta_{CSA}$ | 0.25 *(0.26)* | 0.36 *(0.38)* | 0.06 *(0.07)* | 0.09 *(0.09)* | 0.15 *(0.20)* | 0.05 *(0.07)* |
| d(Mg…N) (Å) | 1.92 *(1.94)* | 1.91 *(1.93)* | 1.97 *(1.97)* | 1.97 *(1.97)* | 1.99 *(2.00)* | 1.98 *(2.00)* |
| d(Mg…Mg) (Å) | - | - | - | - | 2.85 *(2.86)* | 2.85 *(2.86)* |

Values in parenthesis (in italic) were obtained after optimization of all atomic positions, while the other values correspond to H-atom optimization only. d(Mg…N) corresponds to the average Mg…N distance. The equation used to derive calculated shifts from calculated shieldings can be found in supporting information (Figure S2).

**Table 4** DFT-calculated $^{25}$Mg NMR parameters for the "3-coordinate" Mg-organocomplexes shown in Figure 3.

| **CCDC** | **175074** | **266470** | **266468** | **745088** | **661565** |
|---|---|---|---|---|---|
| $\delta_{iso}$ (ppm) | 43.4 *(38.0)* | 54.7 *(53.4)* | 54.8 *(52.7)* | 86.8 *(84.1)* | 70.6 *(69.1)* |
| $C_Q$ (MHz) | −27.36 *(−26.73)* | 27.34 *(26.87)* | 26.81 *(26.12)* | 23.70 *(23.13)* | −24.88 *(−24.53)* |
| $\eta_Q$ | 0.70 *(0.66)* | 0.96 *(0.98)* | 0.86 *(0.85)* | 0.87 *(0.90)* | 0.76 *(0.76)* |
| $\Delta_{CSA}$ (ppm) | −82.3 *(−81.5)* | −91.4 *(−91.6)* | 51.6 *(51.0)* | −88.4 *(−87.9)* | −106.5 *(−105.8)* |
| $\eta_{CSA}$ | 0.27 *(0.28)* | 0.35 *(0.34)* | 0.99 *(0.97)* | 0.59 *(0.59)* | 0.20 *(0.20)* |
| d(Mg…X) (Å) | 2.00 *(2.02)* | 2.04 *(2.05)* | 2.07 *(2.08)* | 2.04 *(2.05)* | 2.07 *(2.09)* |
| d(Mg…Mg) (Å) | - | - | - | 2.81 *(2.80)* | 2.85 *(2.85)* |

Values in parenthesis (in italic) were obtained after optimization of all atomic positions, while the other values correspond to H-atom optimization only. d(Mg…X) corresponds to the average Mg…X distance (X = O, N). The equation used to derive calculated shifts from calculated shieldings can be found in supporting information (Figure S2).

**Table 5** DFT-calculated $^{25}$Mg NMR parameters for the "4-coordinate" Mg-organocomplexes shown in Figure 3.

| **CCDC** | **247151** | **266465** | **266466** | | **266464** |
|---|---|---|---|---|---|
| Site | Mg(1) | Mg(1) | Mg(1) | Mg(1') | Mg(1) |
| $\delta_{iso}$ (ppm) | 34.8 *(29.6)* | 34.8 *(28.9)* | 34.5 *(30.5)* | 36.5 *(31.9)* | 54.1 *(50.5)* |
| $C_Q$ (MHz) | −16.86 *(−16.98)* | −16.83 *(−16.80)* | −15.51 *(−14.88)* | −16.21 *(−15.48)* | −13.93 *(−13.89)* |
| $\eta_Q$ | 0.34 *(0.34)* | 0.34 *(0.35)* | 0.60 *(0.57)* | 0.52 *(0.51)* | 0.51 *(0.51)* |
| $\Delta_{CSA}$ (ppm) | −54.3 *(−55.4)* | −54.3 *(−54.7)* | −42.6 *(−41.8)* | −45.5 *(−44.4)* | −46.5 *(−46.9)* |
| $\eta_{CSA}$ | 0.17 *(0.17)* | 0.17 *(0.18)* | 0.85 *(0.87)* | 0.70 *(0.75)* | 0.57 *(0.56)* |
| d(Mg…X) (Å) | 2.04 *(2.07)* | 2.04 *(2.07)* | 2.10 *(2.12)* | 2.10 *(2.12)* | 2.08 *(2.10)* |

Values in parenthesis (in italic) were obtained after optimization of all atomic positions, while the other values correspond to H-atom optimization only. d(Mg…X) corresponds to the average Mg…X distance (X = O, N). The equation used to derive calculated shifts from calculated shieldings can be found in supporting information (Figure S2).

As in the case of calcium, the calculated isotropic chemical shifts ($\delta_{iso}$ > 30 ppm) and spans ($|\Delta_{CSA}|$ > 40 ppm) were found to be generally higher than those reported in previous experimental $^{25}$Mg NMR studies. The high $\delta_{iso}$ values can be explained by the very short Mg…X distances (Freitas *et al.*, 2009; Freitas *et al.*, 2012; Burgess *et al.*, 2013; Laurencin *et al.*, 2012; Wong *et al.*, 2006). The calculated quadrupolar coupling constants ($|C_Q|$ > 13 MHz) were also found to be very high, and to the best of our knowledge $|C_Q|$ values exceeding 20 MHz had never been reported to date (considering both experimental and computational studies) (Freitas *et al.*, 2012). Such high values can be explained by the very small coordination numbers of Mg within the complexes, which lead to highly unevenly distributed electron densities around the metal ion. It is worth noting that just like in the case of calcium, the CSA span $|\Delta_{CSA}|$ increases globally as a function of $|C_Q|$ (Figure 4a). Moreover, in several cases, the shielding and EFG tensors were found to be co-axial (Figures 4b,d-f). A noticeable exception concerns the Mg-Mg dimer (CCDC 1477718); in this case, the $V_{zz}$ and $\delta_{33}$ components are nearly aligned with the Mg-Mg bond direction (Figure 4c).

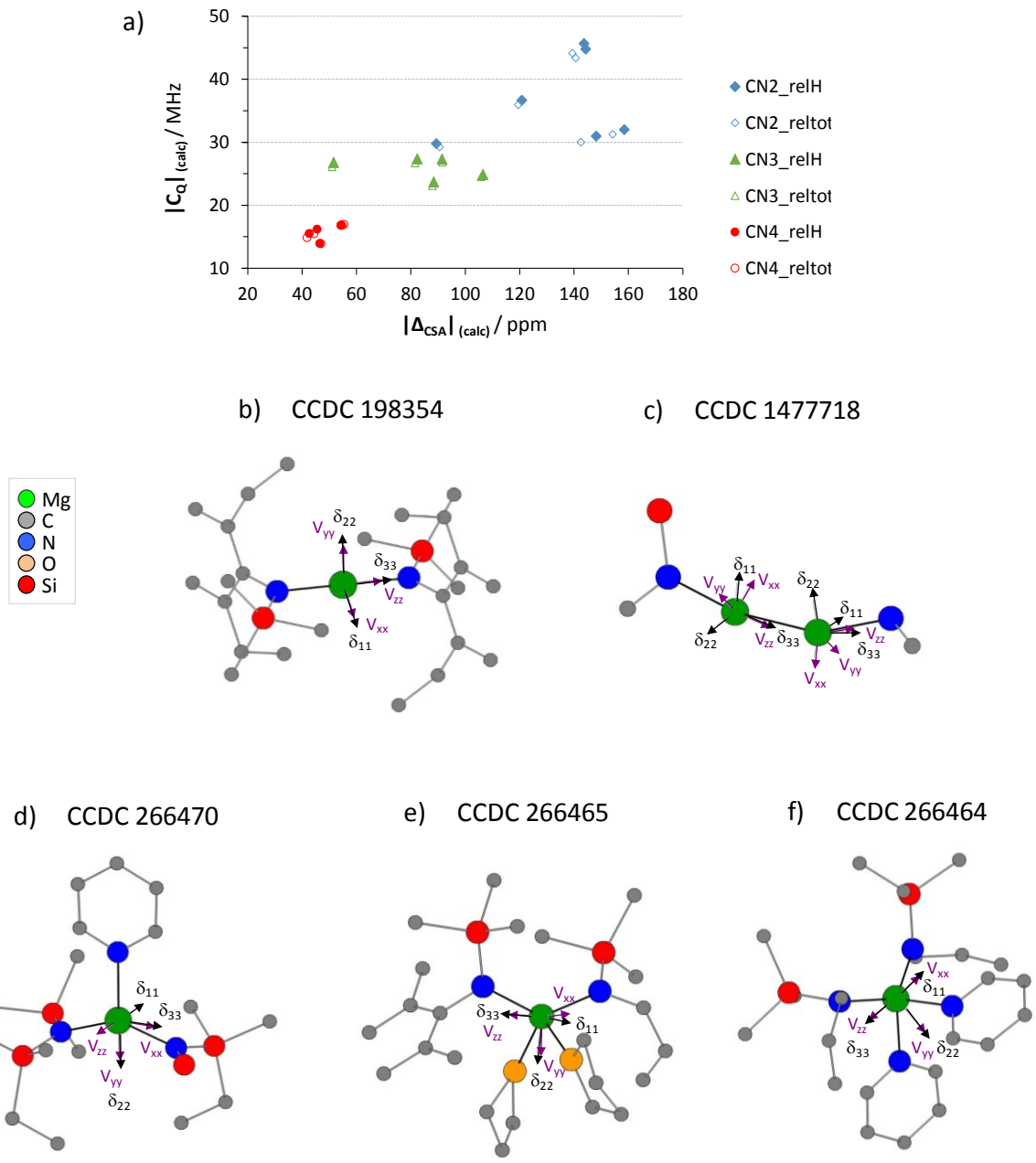


**Figure 4** a) Correlation between $|\Delta_{CSA}|$ and $|C_Q|$ for the organocomplexes shown in Figure 3, depending on the coordination number (CN) of the Mg (CN = 2 in blue, CN = 3 in green, CN = 4 in red). b-f) Relative orientations of the shielding and quadrupolar tensors in structures CCDC 198354, 1477718, 266470, 266465 and 266464 (for clarity, only the non-H atoms within a 5 Å radius around the Mg are shown, except for 1477718 as the figure would have been too complex; Euler angles can be found in Supporting Information – Table S27).

Based on these NMR parameters and the nuclear spin properties of magnesium-25, it appears that experiments performed under MAS conditions would be very difficult to interpret even when working at ultra-high magnetic fields ($B_0 \geq 20$ T), due to the overlap of the sidebands with the central transition resonance. However, under static conditions, using the latest wide-line acquisition methods (Schurko, 2013), it should be possible to record the static spectra of these compounds. Some of the possible methods include the VOCS-WURST-QCPMG sequence (Variable-Offset Cumulative Spectroscopy – Wideband, Uniform Rate, Smooth Truncation – Quadrupolar Carr Purcell Meiboom Gill), with additional $^{1}$H decoupling to increase the transverse relaxation rates. Such experiments will be challenging, as shown by the simulations of the expected spectra at 20 T (see supporting information, Figure S6), the full breadth of the central transition signal exceeding 1 MHz in some cases. This implies that isotopic enrichment in $^{25}$Mg will most probably be needed to obtain high quality spectra. Due to the very large $|C_Q|$ values, it appears that it will not be possible to determine the CSA parameters from the static spectra (see supporting information, Figure S6), but it should be possible to extract $|C_Q|$ and $\eta_Q$ values. Nevertheless, it is worth noting that in cases when there are two different Mg sites with similar local environments (compounds 198354 (Figure 3a) and 1477718 (Figure 3d)), the calculated NMR parameters are very close, with for example $|C_Q|$ values differing by less than 1 MHz. This implies that resolving the 2 crystallographic sites using $^{25}$Mg NMR may be very difficult experimentally. An alternate way to measure the quadrupolar parameters could be to perform NQR (nuclear quadrupolar resonance) characterizations at different temperatures.

When comparing the different structures studied here, it appears that $|C_Q|$ globally increases as the coordination number decreases from 4 to 2 (Figure 5). Calculations on more species would of course be needed to further confirm these trends, and to include other Mg local environments such as 4-coordinate Mg compounds in which the metal ion lies in the same plane as the 4 atoms to which is it bound. Nevertheless, from the data presented here, as a first approximation, it could be tempting to suggest that the measurement of $|C_Q|$ can be used as a guideline for determining the Mg coordination number in complex *low-coordinate* structures, and notably those in which only powder X-ray diffraction data of poor quality is available. However, previous studies on 5- and 6-coordinate Mg(II) complexes show that it may not always be so simple. Indeed, while $|C_Q|$ values are generally much lower than 12 MHz in 5- and 6-coordinate complexes (Freitas *et al.*, 2009), i.e. below those observed here for the 4-coordinate compounds, noticeable exceptions exist for porphyrin or phtalocyanine Mg-complexes, in which the metal ion sits in the cavity of the macrocycle, with distorted octahedral (CN = 6) or square pyramidal (CN = 5) environments. Indeed, $|C_Q|$ values were observed in the ~13-15 MHz range for these systems (Wu *et al.*, 2003; Wong *et al.*, 2006), which is close to what we have found for 4 coordinate complexes. Therefore, the $|C_Q|$ parameter should be considered carefully, when it comes to predicting Mg coordination numbers.

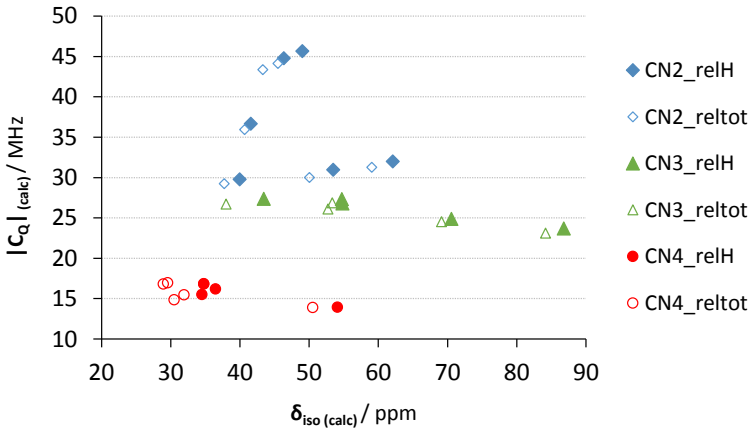


**Figure 5** Representation of the variations in calculated $\delta_{iso}$ and $|C_Q|$ parameters as a function of the coordination number, for the Mg complexes shown in Figure 3.

The lowest-coordination Mg(II) complexes (Figures 3a-3c) are worth discussing in more detail. Indeed, despite the overall similarity in coordination environment of the Mg(II), significant variations in average Mg…X distances and even more in N-Mg-N bond angles, are actually observed, due to the change in the bulkiness of the organic groups directly linked to the N atoms. This has a direct impact on the calculated $|C_Q|$ values, which vary by more than 15 MHz between the 3 systems. It is noted that for these compounds, the smaller the N-Mg-N bond angle, the smaller the $|C_Q|$. The 4-coordinate Mg complexes are also interesting to discuss (Figures 3j-3l). Indeed, while only small differences in calculated $\delta_{iso}$ and $|C_Q|$ values are observed for compounds 3j and 3k, more significant changes were found for compound 3l, which reflects the fact that the local geometry around the Mg in this complex is more different than in the other two, in terms of N-Mg-X bond angles. Overall, these observations underscore the very high sensitivity of $^{25}$Mg NMR to changes in local environments of the metal, and hence its potential utility for assisting in the refinement of crystallographic data, or even to understand the structure of non-crystalline/disordered structures.

## 4. Conclusion

In this manuscript, we have described the first $^{25}$Mg and $^{43}$Ca NMR computational study of a series of *low-coordination* Mg and Ca complexes (CN = 2 to 4), which are of interest in organometallic chemistry and catalysis. By focusing on the calculated NMR parameters of the metal ions, it was demonstrated how the combination of solid state NMR and GIPAW calculations of NMR parameters can be useful for assisting in the resolution and/or refinement of complex crystal structures. The $^{43}$Ca chemical shifts and $^{25}$Mg quadrupolar parameters were indeed found to be very sensitive to small changes in the coordination environment of the metal ions.

The NMR parameters calculated in this study expand by far the ranges of values reported so far for these nuclei. Particularly large quadrupolar coupling constants $|C_Q|$ and chemical shift anisotropies $|\Delta_{CSA}|$ were notably calculated for both $^{43}$Ca and $^{25}$Mg, and the consequences on the measurement conditions to use for the NMR experiments were discussed. In particular, considering the current instruments and pulse sequences currently available, isotopic enrichment in $^{43}$Ca or $^{25}$Mg will be needed to ensure the acquisition of high quality spectra. Considering the cost of the isotopically-labeled $^{25}$Mg and $^{43}$Ca precursors, it will unfortunately not be possible to perform such experiments on a routine basis.

Attempts were made to correlate the calculated NMR parameters of $^{43}$Ca and $^{25}$Mg to a structural feature around the metal ion, for example its coordination number. The general observation was that $|C_Q|$ increased as the coordination number decreased from 4 to 3 (in the case of Ca), or 4 to 2 (in the case of Mg). However, it was shown on the basis of previously published data that this trend needs to be taken very carefully, because in some cases relatively large $|C_Q|$ values can also be found for higher coordination numbers if the coordination polyhedron is distorted. It is worth noting that for other s-block metal cations like $Sr^{2+}$ and $Na^+$, it has also been shown that it can be very difficult to relate the $|C_Q|$ values to a given coordination number (Bonhomme *et al.*, 2012b; Wong *et al.*, 2000). Overall, this indicates that it is only through the combination of NMR experiments and DFT calculations that it will be possible to establish the coordination environment of Ca and Mg, and subsequently use this information as a support to X-ray structure determination.

**Acknowledgements** NMR spectroscopic calculations were performed using HPC resources from GENCI-IDRIS (Grant 2016-097535). The CNRS and the Embassy of France in Australia are acknowledged for financial support.

## References

Avent, A. G., Crimmin, M. R., Hill, M. S. & Hitchcock, P. B. (2005) *Dalton Trans.* 278-284.

Barrett, A. G. M., Crimmin, M. R., Hill, M. S., Kociok-Köhn, G., MacDougall, D. J., Mahon, M. F. & Procopiou, P. P. (2008) *Organometallics*, **27**, 939-3946.

Bartlett, R. A., Olmstead, M. M. & Power, P. P. (1994) *Inorg. Chem.* **33**, 4800-4803.

Bonhomme, C., Gervais, C., Babonneau, F., Coelho, C., Pourpoint, F., Azaïs, T., Ashbrook, S. E., Griffin, J. M., Yates, J. R., Mauri, F. & Pickard, C .J. (2012a) *Chem. Rev.* **112**, 5733–5779.

Bonhomme, C., Gervais, C., Folliet, N., Pourpoint, F., Coelho Diogo, C., Lao, J., Jallot, E., Lacroix, J., Nedelec, J.-M., Iuga, D., Hanna, J. V., Smith, M. E., Xiang, Y., Du, Y. & Laurencin, D. (2012b) *J. Am. Chem. Soc.* **134**, 12611−12628.

Bonyhady, S. J., Jones, C., Nembenna, S., Stasch, A., Edwards, A. J. & McIntyre, G. J. (2010) *Chem. Eur. J.* **16**, 938-955.

Boutland, A. J., Dange, D., Stasch, A., Maron, L. & Jones, C. (2016) *Angew. Chem. Int. Ed.* **55**, 9239-9243.

Burgess, K. M. N., Xu, Y.; Leclerc, M. C. & Bryce, D. L. (2013) *J. Phys. Chem. A*, **117**, 6561-6570.

Burgess, K. M. N., Xu, Y.; Leclerc, M. C. & Bryce, D. L. (2014) *Inorg. Chem.* **53**, 552-561.

Cahill, L. S., Hanna, J. V., Wong, A., Freitas, J. C. C., Yates, J. R., Harris, R. K. & Smith, M. E. (2009) *Chem.-Eur. J.* **15**, 9785−9798.

Ceresoli, D. 2012, https://sites.google.com/site/dceresoli/pseudopotentials.

Freitas, J. C. C., Wong, A. & Smith, M. E. (2009) *Magn. Reson. Chem.* **47**, 9-15.

Freitas, J. & Smith, M. E. (2012) *Annu. Rep. NMR Spectrosc.* **75**, 25−114.

Gambuzzi, E., Pedone, A., Menziani, M. C., Angeli, F., Florian, P., Charpentier, T. (2015) *Solid St. Nucl. Magn. Reson.* **68-69**, 31–36.

Gervais, C., Laurencin, D., Wong, A., Pourpoint, F., Labram, J., Woodward, B., Howes, A. P., Pike, K. J., Dupree, R., Mauri, F., Bonhomme, C. & Smith, M. E. (2008) *Chem. Phys. Lett.* **464**, 42-48.

Harder, S. (2013) "Alkaline-earth metal compounds: oddities and applications." in *Topics Organomet. Chem.* **45**:

Giannozzi, P. *et al.* (2009) *J. Phys.: Condens. Matter*, **21**, 395502.

Gillett-Kunnath, M., Teng, W., Vargas, W. & Ruhlandt-Senge, K. (2005) *Inorg. Chem.* 44, 4862-4870.

Gras, P., Baker, A., Combes, C., Rey, C., Sarda, S., Wright, A. J., Smith, M. E., Hanna, J. V., Gervais, C., Laurencin, D. & Bonhomme, C. (2016) *Acta Biomater.* **31**, 348-357.

Green, S. P., Jones, C. & Stasch, A. (2007) *Science*, **318**, 1754-1757.

Haeberlen, U. (1976), *Advances in Magnetic Resonance*, Suppl. 1; J. S. Waugh, Ed.; Academic Press: New York (see http://anorganik.uni-tuebingen.de/klaus/nmr/index.php?p=conventions/csa/csa#6).

Harris, R. K., Wasylishen, R. E. & Duer, M. J. (2009), *NMR Crystallography*, Wiley VCH.

Kennedy, A. R., Mulvey, R. E. & Schulte, J. H. (2001), *Acta Cryst*. **C57**, 1288-1289.

Kleinman, L. & Bylander, D. (1982) *Phys. Rev. Lett.* **48**, 1425-1428.

Kobayashi, S., Yamashita, Y. (2011), *Acc. Chem. Res*. **44**, 58-71.

Komorovsky, S., Repisky, M., Malkin, E., Ruud, K. & Gauss, J. (2015) *J. Chem. Phys.* **142**, 091102.

Laurencin, D., Gervais, C., Stork, H., Kraemer, S., Massiot, D. & Fayon, F. (2012) *J. Phys. Chem. C*, **116**, 19984−19995.

Laurencin, D. & Smith, M. E. (2013) *Prog. Nucl. Magn. Reson. Spectrosc.* **68**, 1-40.

Lejaeghere, K., Bihlmayer, G., Björkman, T., Blaha, P., Blügel, S., Blum, V., Caliste, D., Castelli, I. E., Clark, S. J., Dal Corso, A., de Gironcoli, S., Deutsch, T. & *al*, (2016) *Science*, **351**, 1415.

Massiot, D., Fayon, F., Capron, M., King, I., Le Calvé, S., Alonso, B., Durand, J. O., Bujoli, B., Gan, Z. & Hoatson, G. (2002) *Magn. Reson. Chem.* **40**, 70-76.

Murgia, F., Stievano, L., Monconduit, L. & Berthelot, R. (2015) *J. Mater. Chem. A*, **3**, 16478-16485.

Pallister, P. J., Moudrakovski, I. L. & Ripmeester, J. A. (2009) *Phys. Chem. Chem. Phys.* **11**, 11487−11500.

Perdew, J. P., Burke, K. & Ernzerhof, M. (1996) *Phys. Rev. Lett.* **77**, 3865-3868.

Perras, F. A., Widdifield, C. M. & Bryce, D. L. (2012) *Solid St. Nucl. Magn. Reson.* **45-46**, 36-44.

Perras, F. A.; Viger-Gravel, J.; Burgess, K. M. N. & Bryce, D. L. (2013) *Solid St. Nucl. Magn. Reson.* **51-52**, 1-15.

Pickard, C. & Mauri, F. (2001) *Phys. Rev. B*, **63**, 245101.

Pyykkö, P. (2008) *Mol. Phys.* **106**, 1965-1974.

Sarrazin, Y. & Carpentier, J.-F. (2016) *The Chemical Record,* doi:10.1002/tcr.201600067.

Schurko, R. W. (2013) *Acc. Chem. Res.* **46**, 1985–1995.

Schurko, R. W. & Jaroszewicz, M. J. (2015). Solid-State NMR of the Light Main Group Metals. In "The Lightest Metals", Encyclopedia of Inorganic and Bioinorganic Chemistry, John Wiley & Sons, New York, 117-172.

Sene, S., Bouchevreau, B., Martineau, C., Gervais, C., Bonhomme, C., Gaveau, P., Mauri, F., Bégu, S., Mutin, P. H., Smith, M. E. & Laurencin, D. (2013) *CrystEngComm,* **15**, 8763-8775.

Sene, S., Bégu, S., Gervais, C., Renaudin, G., Mesbah, A., Smith, M. E., Mutin, P. H., van der Lee, A., Nedelec, J.-M., Bonhomme, C. & Laurencin, D. (2015), *Chem. Mater.* **27**, 1242-1254.

Soulié, J., Gras, P., Marsan, O., Laurencin, D., Rey, C. & Combes, C. (2016) *Acta Biomater*. **41**, 320-327.

Sowrey, F. E., Skipper, L. J., Pickup, D. M., Drake, K. O., Lin, Z., Smith, M. E., Newport, R. J. (2004) *Phys. Chem. Chem. Phys*.**6**, 188-192.

Tang, Y., Zakharov, L. N., Kassel, W. S., Rheingold, A. L. & Kemp, R. A. (2005a) *Inorg. Chim. Acta*, **358**, 2014-2022.

Tang, Y., Zakharov, L. N., Rheingold, A. L. & Kemp, R. A. (2005b) *Organometallics*, **24**, 836-841.

Torvisco, A., O'Brien, A. Y. & Ruhlandt-Senge, K. (2011) *Coord. Chem. Rev.* **255**, 1268-1292.

Troullier, N. & Martins, J. L. (1991) *Phys. Rev. B* **43**, 1993-2006.

Vargas, V., Englich, U. & Ruhlandt-Senge, K. (2002) *Inorg. Chem.* **41**, 5602-5608.

Widdifield, C. M., Moudrakovski, I. & Bryce, D. L. (2014) *Phys. Chem. Chem. Phys.* **16**, 13340-13359.

Wong, A. & Wu, G. (2000) *J. Phys. Chem. A*, **104**, 11844-11852.

Wong, A., Ida, R., Mo, X., Gan, Z., Poh, J. & Wu, G. (2006) *J. Phys. Chem. A,* **110**, 10084-10090.

Wong, A., Laurencin, D., Wu, G., Dupree, R., Smith, M. E., (2008) *J. Phys. Chem. A*, **112**, 9807-9813.

Wu, G., Wong, A. & Wang, S. (2003) *Can. J. Chem.*, **81**, 275.

# Supporting information

### S1. Additional DFT calculations on organocalcium and organomagnesium complexes

**Table S1** DFT calculations on magnesium complex CCDC 198354: influence of the k-point mesh, the energy cut-off, and the optimization of unit cell parameters.

| **Optimization** | **H atoms** | | **H atoms** | | **H atoms** | | **All atoms** | | **All atoms + cell parameters** | |
|---|---|---|---|---|---|---|---|---|---|---|
| k-point grid | (1x1x1) | | (1x1x1) | | (2x2x2) | | (1x1x1) | | (1x1x1) | |
| Energy cut-off (Ry) | 60 | | 80 | | 60 | | 80 | | 80 | |
| Site | Mg(1) | Mg(2) | Mg(1) | Mg(2) | Mg(1) | Mg(2) | Mg(1) | Mg(2) | Mg(1) | Mg(2) |
| $\delta_{iso}$ (ppm) | 46.3 | 49.0 | 46.3 | 49.0 | 50.0 | 50.7 | 43.3 | 45.5 | 43.7 | 45.0 |
| $C_Q$ (MHz) | −44.80 | −45.69 | −44.79 | −45.68 | −44.70 | −45.71 | −43.36 | −44.15 | −43.59 | −44.39 |
| $\eta_Q$ | 0.23 | 0.23 | 0.23 | 0.23 | 0.24 | 0.22 | 0.24 | 0.23 | 0.24 | 0.23 |

**Table S2** DFT calculations on Mg and Ca complexes 198354, 266468, 745088 and 255195: influence of the dispersion correction.

| **CCDC** | **198354** | | | | **266468** | | **745088** | | **255195** | |
|---|---|---|---|---|---|---|---|---|---|---|
| Optimization | All atoms | | All atoms | | All atoms | | All atoms | | All atoms | |
| k-point grid | (1x1x1) | | (1x1x1) | | (1x1x1) | | (1x2x1) | | (1x1x1) | |
| Energy cut-off (Ry) | 80 | | 60 | | 60 | | 80 | | 80 | |
| Dispersion | - | | yes | | - | yes | - | yes | - | yes |
| Site | Mg(1) | Mg(2) | Mg(1) | Mg(2) | Mg(1) | Mg(1) | Mg(1) | Mg(1) | Ca(1) | Ca(1) |
| $\delta_{iso}$ (ppm) | 43.3 | 45.5 | 43.0 | 44.6 | 52.7 | 55.1 | 84.1 | 84.2 | 103.3 | 110.5 |
| $C_Q$ (MHz) | −43.36 | −44.15 | −43.13 | −43.58 | 26.12 | 27.07 | 23.13 | 23.12 | −6.11 | −6.17 |
| $\eta_Q$ | 0.24 | 0.23 | 0.24 | 0.23 | 0.85 | 0.84 | 0.90 | 0.88 | 0.85 | 0.86 |

**Table S3** DFT calculations on calcium complex CCDC 247152: influence of the k-point mesh.

| **k-point grid** | **(1x1x1)** | **(2x2x2)** |
|---|---|---|
| $\delta_{iso}$ (ppm) | 102.1 | 102.1 |
| $C_Q$ (MHz) | 7.22 | 7.22 |
| $\eta_Q$ | 0.15 | 0.15 |

GIPAW calculations reported here were performed using an energy cut-off of 80 Ry and correspond to H-atom optimization only.

## S2. Calibration of $^{43}$Ca and $^{25}$Mg NMR parameter calculations

**Table S4** DFT-calculated $^{43}$Ca NMR shieldings of a selection of crystalline phases, used for the calibration of $^{43}$Ca NMR calculations, together with the previously reported experimental $^{43}$Ca isotropic chemical shifts.

| Structure | $\sigma_{(iso)}$ (calc) / ppm | $\delta_{(iso)}$ (exp) / ppm |
|---|---|---|
| CaO | 951.8 | 136 (1) |
| $Ca(OH)_2$ | 1027.2 | 71 (3) |
| $CaCO_3$ (calcite) | 1100.0 | 22 (2) |
| $CaCO_3$ (aragonite) | 1137.8 | −26 (1) |
| Hydroxyapatite | 1115.4 | 4.5 (1) |
| | 1095.4 | 17.5 (1) |
| $Ca(H_2PO_4)_2.H_2O$ | 1136.5 | −15 (5) |
| $CaB_2O_4$ | 1109.4 | 6 (5) |
| $CaAl_4O_7$ | 1055.6 | 54 (5) |
| α-$Ca_2P_2O_7$ | 1145.7 | −18 (5) |
| | 1111.1 | 12 (5) |

Experimental values taken from Laurencin, D. *et al* (2013) *Prog. Nucl. Magn. Reson. Spectrosc.* **68**, 1−40.

**Figure S1** Plots of $\sigma_{iso}$(calc) as a function of $\delta_{iso}$(exp) (left), and $P_Q$(calc) as a function of $P_Q$(exp) (right), for the calcium compounds shown in Table S4 ($P_Q = C_Q(1 + \eta_Q^2/3)^{0.5}$)).

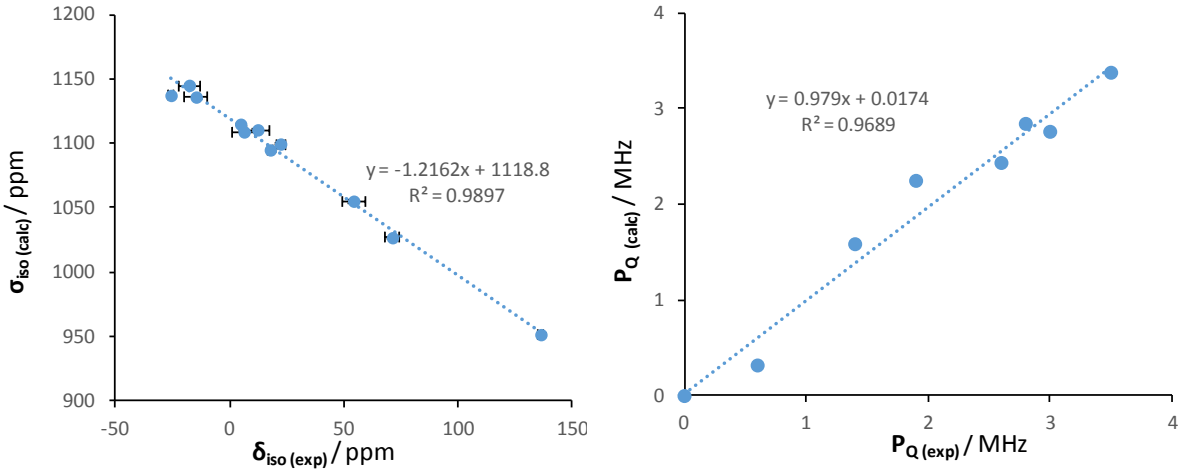

**Table S5** DFT-calculated $^{25}$Mg NMR shieldings and $|C_Q|$ values of a selection of crystalline phases, used for the calibration of $^{25}$Mg NMR calculations, together with the previously reported experimental $^{25}$Mg isotropic chemical shifts and $|C_Q|$ values (experimental errors are given in parenthesis).

| Structure | ICSD | $\sigma_{(iso)}$ (calc) / ppm | $\delta_{(iso)}$ (exp) / ppm | $\|C_Q\|$ (calc) / MHz | $\|C_Q\|$ (exp) / MHz |
|---|---|---|---|---|---|
| MgO | 52026 | 541.3 | 26.26 (5) [a] | | |
| $Mg(OH)_2$ | 203212 | 553.4 | 11.8 (2) [a] | 2.95 | 3.09(1) |
| $MgCO_3$ | 73731 | 566.2 | −3.8 (2) [a] | 1.29 | 2.24(2) |
| α-$Mg_2P_2O_7$ | 15326 | 577.5 | −11 (1) [b] | 3.96 | 4.05 (4) |
| | | 566.5 | −6 (3) [b] | 11.76 | 12.45 (4) |
| $Mg(PO_3)_2$ | 4280 | 580.9 | −10 (1) [b] | 3.42 | 3.09 (4) |
| | | 571.5 | −2 (2) [b] | 4.38 | 4.62 (6) |
| $Mg_3(PO_4)_2$ | 31005 | 554.7 | 17 (2) [b] | 7.08 | 7.12 (2) |
| | | 578.0 | −4 (2) [b] | 6.95 | 5.77 (6) |

Experimental values taken from [a] Pallister, P. J. *et al* (2009), *Phys. Chem. Chem. Phys.* **11**, 11487–11500, and [b] Laurencin, D. *et al* (2012) *J. Phys. Chem. C*, **116**, 19984−19995.

**Figure S2** Plots of $\delta_{iso}$(exp) as a function of $\sigma_{iso}$(calc) (left), and $|C_Q$(calc)| as a function of $|C_Q$(exp)| (right), for the magnesium compounds shown in Table S5.

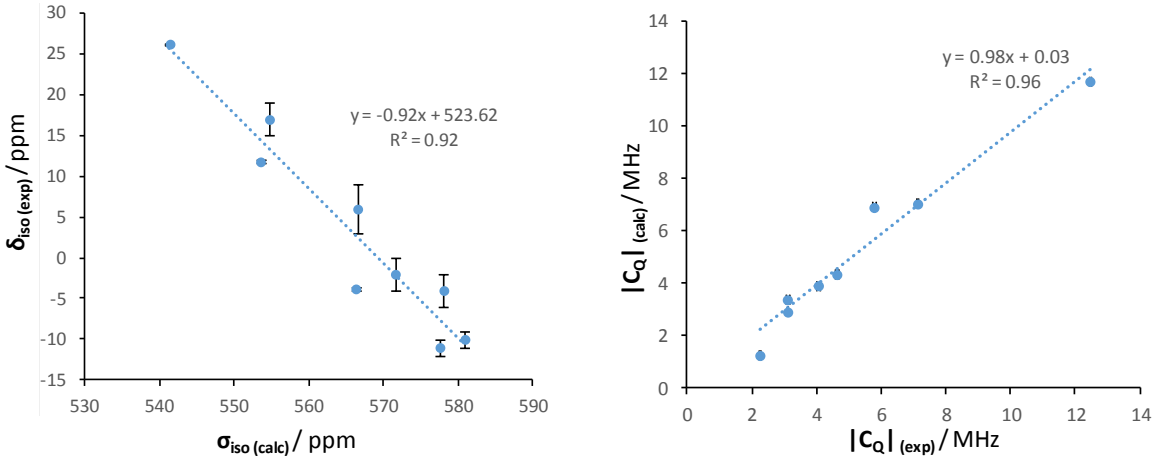

### S3. Local environments of calcium in the organocomplexes studied by DFT

**Table S6** Closest neighbors around the 2 calcium sites (within a 3.0 Å radius) in the organocalcium structure CCDC 255198.

| | **H-optimization** | **Full -optimization** |
|---|---|---|
| Ca Neighbor | Distance (Å) | Distance (Å) |
| N | 2.32 | 2.34 |
| N | 2.33 | 2.34 |
| O | 2.38 | 2.43 |
| H | 2.67 | 2.68 |
| C | 2.86 | 2.86 |
| H | 2.86 | 2.90 |

**Table S7** Closest neighbors around the 2 calcium sites (within a 3.0 Å radius) in the organocalcium structure CCDC 704097.

| | **H-optimization** | **Full -optimization** |
|---|---|---|
| Ca Neighbor | Distance (Å) | Distance (Å) |
| N | 2.29 | 2.29 |
| N | 2.29 | 2.29 |
| C | 2.60 | 2.61 |
| H | 2.76 | 2.78 |
| H | 2.76 | 2.78 |

**Table S8** Closest neighbors around the calcium (within a 3.0 Å radius) in the organocalcium structure CCDC 255195.

| | **H-optimization** | **Full optimization** |
|---|---|---|
| Ca Neighbor | Distance (Å) | Distance (Å) |
| N | 2.35 | 2.33 |
| N | 2.36 | 2.37 |
| N | 2.52 | 2.53 |
| N | 2.55 | 2.57 |
| H | 2.73 | 2.74 |
| H | 2.76 | 2.77 |
| H | 2.83 | 2.84 |
| C | 2.94 | 2.95 |

**Table S9** Closest neighbors around the calcium (within a 3.0 Å radius) in the organocalcium structure CCDC 255196.

| | **H-optimization** | **Full optimization** |
|---|---|---|
| Ca Neighbor | Distance (Å) | Distance (Å) |
| N | 2.36 | 2.37 |
| N | 2.37 | 2.39 |
| N | 2.47 | 2.50 |
| N | 2.52 | 2.57 |
| H | 2.66 | 2.67 |
| H | 2.87 | 2.90 |
| H | 2.89 | 2.97 |
| C | 2.98 | 2.99 |

**Table S10** Closest neighbors around the 2 calcium sites (within a 3.0 Å radius) in the organocalcium structure CCDC 198356.

| | **H-optimization** | **Full -optimization** |
|---|---|---|
| Ca(1) Neighbor | Distance (Å) | Distance (Å) |
| N | 2.33 | 2.35 |
| N | 2.33 | 2.35 |
| O | 2.35 | 2.39 |
| O | 2.37 | 2.44 |
| C | 2.95 | 2.98 |
| C | 2.98 | 2.99 |
| | | |
| Ca(2) Neighbor | Distance (Å) | Distance (Å) |
| N | 2.32 | 2.34 |
| N | 2.33 | 2.36 |
| O | 2.35 | 2.40 |
| O | 2.36 | 2.41 |
| C | 2.84 | 2.87 |

**Table S11** Closest neighbors around the calcium (within a 3.0 Å radius) in the organocalcium structure CCDC 247152.

| | **H-optimization** | **Full optimization** |
|---|---|---|
| Ca Neighbor | Distance (Å) | Distance (Å) |
| N | 2.30 | 2.31 |
| N | 2.31 | 2.32 |
| O | 2.34 | 2.39 |
| O | 2.35 | 2.41 |
| H | 2.97 | 2.87 |

### S4. Simulation of $^{43}$Ca NMR spectra based on the GIPAW calculated NMR parameters

**Figure S3** Simulation of the $^{43}$Ca MAS NMR spectra at 20 T, for structures CCDC 198356 (Ca (1) site) and 704097, based on the values calculated in Tables 1 and 2 for the H-relaxed structures. Simulations were performed assuming an "infinite" spinning speed; only central transitions are represented here.

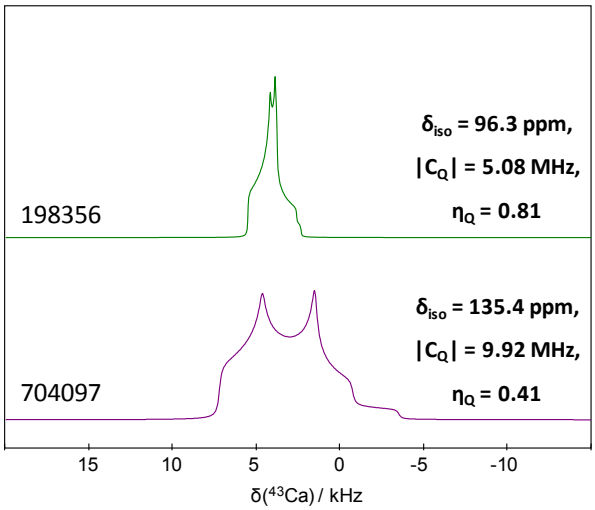


**Table S12** Calculated $^{43}$Ca NMR parameters after H-optimization of structures CCDC 255198, 704097 and 247152.

| | **255198** | **704097** | **247152** |
|---|---|---|---|
| $\delta_{iso}$ (ppm) | 99.5 | 135.4 | 102.1 |
| $\|C_Q\|$ (MHz) | 8.0 | 9.9 | 7.2 |
| $\eta_Q$ | 0.8 | 0.4 | 0.2 |
| $\Omega$ (ppm) | 286.5 | 310.2 | 224.6 |
| $\kappa$ | 0.3 | −0.7 | 0.8 |
| $\alpha$ | −100 | 90 | 115 |
| $\beta$ | 175 | −90 | 175 |
| $\gamma$ | 0 | 0 | 5 |

The relative orientation between the two tensors using three Euler angles ($\alpha$,$\beta$,$\gamma$) was extracted from the first-principles calculations, which allows the simulation of the static spectra taking all these parameters into account. The QUEST software was used to simulate these spectra (Figure S4). The Euler angles reported therefore describe the relative orientation of the EFG tensor with respect to the shielding tensor along the following conventions : $\delta_{11} \geq \delta_{22} \geq \delta_{33}$ and $|V_{33}| \geq |V_{22}| \geq |V_{11}|$). Span $\Omega = \delta_{11} - \delta_{33}$ and skew $\kappa = 3(\delta_{22} - \delta_{iso})/ \Omega$.

**Figure S4** Simulation of the static $^{43}$Ca NMR spectra at 20 T, for structures CCDC 255198, 704097 and 247152, using the QUEST program. The NMR parameters calculated in Tables 1 and 2 for the H-relaxed structures were used. Only central transitions are represented here. Euler angles are given in Table S12 (above). The relative orientation of shielding and EFG tensors is shown in Figure 2. The simulations were performed with (a) and without (b) the shielding tensor, showing that for $^{43}$Ca, it is necessary to take shielding tensors into account to properly interpret the static lineshape at high field.

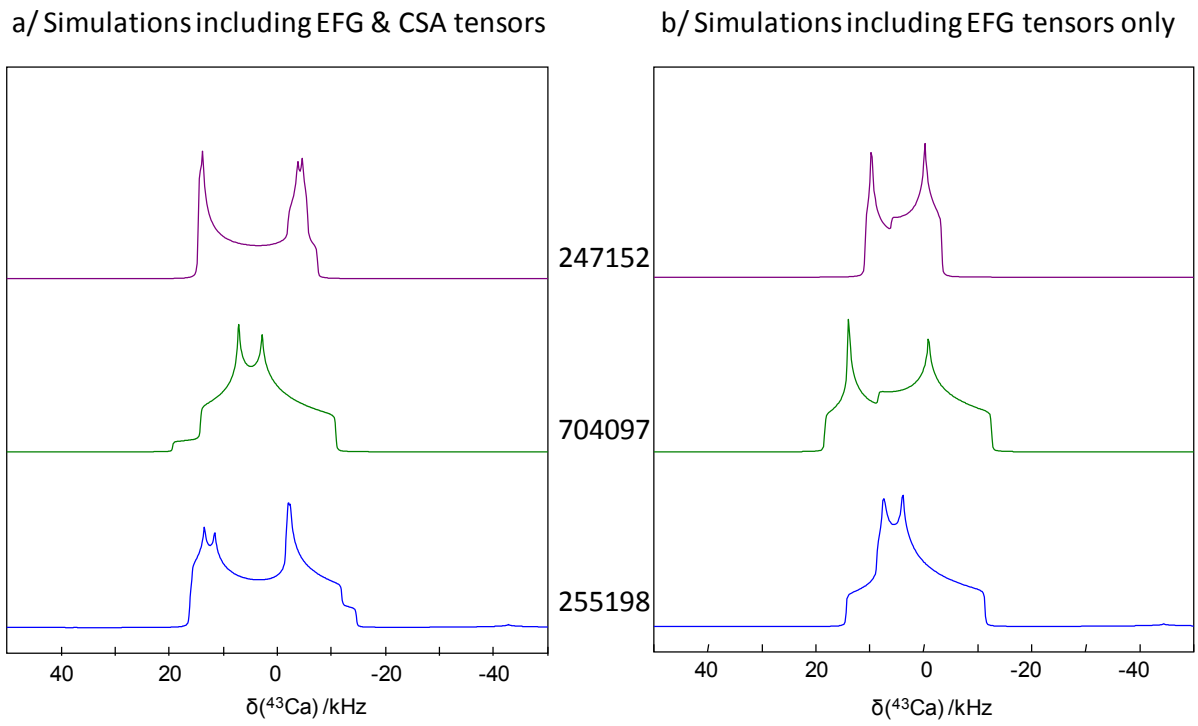

**S5. Local environments of calcium in a penta-coordinated diketiminato complex**

**Figure S5** Representation of the Ca local environment in the crystal structure CCDC 244505.

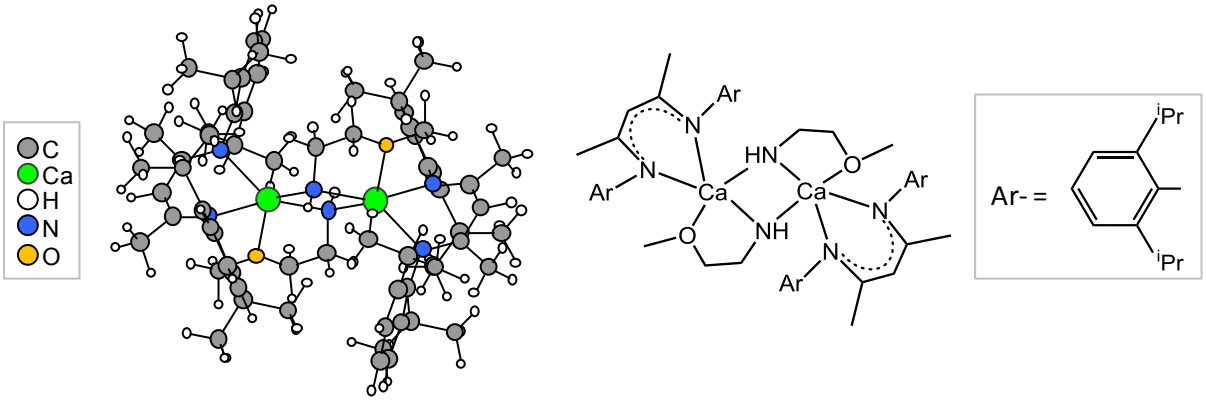


**Table S13** Calculated $^{43}$Ca NMR parameters after H-optimization or full optimization of structure CCDC 244505.

| | **H-optimization** | **Full optimization** |
|---|---|---|
| $\delta_{iso}$ (ppm) | 117.0 | 101.9 |
| $C_Q$ (MHz) | −7.13 | −6.68 |
| $\eta_Q$ | 0.62 | 0.66 |
| $\Delta_{CSA}$ (ppm) | 62.9 | 64.3 |
| $\eta_{CSA}$ | 0.78 | 0.68 |
| d(Ca…X) (Å) | 2.41 | 2.45 |

d(Ca…X) corresponds to the average Ca…X distance (X = N, O). The equation used to derive calculated shifts from calculated shieldings can be found in supporting information (Figure S1).

**Table S14** Closest neighbors around the calcium (within a 3.0 Å radius) in the organocalcium structure CCDC 244505.

| **H-optimization** | | **Full optimization** | |
|---|---|---|---|
| Ca Neighbor | Distance (Å) | Ca Neighbor | Distance (Å) |
| N | 2.37 | N | 2.40 |
| N | 2.40 | N | 2.44 |
| N | 2.41 | N | 2.45 |
| O | 2.43 | N | 2.46 |
| N | 2.43 | O | 2.49 |
| H | 2.91 | H | 2.94 |
| H | 2.93 | H | 2.99 |

**S6. Local environments of magnesium in the organocomplexes studied by DFT.**

**Table S15** Closest neighbors around the 2 Mg sites (within a 3.0 Å radius) in the organomagnesium structure CCDC 198354 (H-optimized structure).

| **Rel H** | | **Rel tot** | | **Rel H** | | **Rel tot** | |
|---|---|---|---|---|---|---|---|
| **Mg(1) site** | | | | **Mg(2) site** | | | |
| Neighbor | Dist. (Å) | Neighbor | Dist. (Å) | Neighbor | Dist. (Å) | Neighbor | Dist. (Å) |
| N | 1.92 | N | 1.94 | N | 1.91 | N | 1.93 |
| N | 1.92 | N | 1.94 | N | 1.91 | N | 1.93 |
| H | 2.82 | H | 2.84 | H | 2.65 | H | 2.67 |
| H | 2.82 | H | 2.84 | H | 2.65 | H | 2.67 |
| H | 2.85 | H | 2.85 | H | 2.69 | H | 2.69 |
| H | 2.85 | H | 2.85 | H | 2.69 | H | 2.69 |
| H | 2.88 | H | 2.90 | C | 2.86 | C | 2.86 |
| H | 2.88 | H | 2.90 | C | 2.86 | C | 2.86 |
| C | 2.94 | C | 2.94 | C | 2.97 | C | 2.98 |
| C | 2.94 | C | 2.94 | C | 2.97 | C | 2.98 |
| H | 2.97 | H | 2.98 | | | | |
| H | 2.97 | H | 2.98 | | | | |
| C | 2.98 | C | 2.99 | | | | |
| C | 2.98 | C | 2.99 | | | | |

**Table S16** Closest neighbors around the calcium (within a 3.0 Å radius) in the organomagnesium structure CCDC 1207191.

| | **H-optimization** | **Full optimization** |
|---|---|---|
| Mg Neighbor | Distance (Å) | Distance (Å) |
| N | 1.96 | 1.97 |
| N | 1.97 | 1.98 |
| C | 2.65 | 2.66 |
| H | 2.69 | 2.75 |
| C | 2.82 | 2.83 |
| C | 2.92 | 2.91 |
| Si | 2.93 | 2.93 |
| C | 2.96 | 2.96 |

**Table S17** Closest neighbors around the calcium (within a 3.0 Å radius) in the organomagnesium structure CCDC 266469.

| **H-optimization** | | **Full optimization** | |
|---|---|---|---|
| Mg Neighbor | Distance (Å) | Mg Neighbor | Distance (Å) |
| N | 1.98 | N | 1.99 |
| N | 1.99 | N | 2.00 |
| H | 2.53 | H | 2.48 |
| C | 2.56 | C | 2.58 |
| C | 2.65 | C | 2.65 |
| C | 2.79 | C | 2.86 |
| Si | 2.89 | Si | 2.91 |
| C | 2.94 | C | 2.93 |
| H | 2.95 | | |
| Si | 2.98 | | |

**Table S18** Closest neighbors around the calcium (within a 3.0 Å radius) in the organomagnesium structure CCDC 266469.

| **H-optimization** | | **Full optimization** | |
|---|---|---|---|
| **Mg(1) site** | | | |
| Mg(1) Neighbor | Distance (Å) | Mg (1) Neighbor | Distance (Å) |
| N | 1.99 | N | 2.00 |
| H | 2.74 | C | 2.73 |
| C | 2.77 | H | 2.75 |
| Mg | 2.85 | Mg | 2.86 |
| H | 2.92 | H | 2.89 |
| C | 2.93 | C | 2.93 |
| C | 2.96 | H | 2.99 |
| | | | |
| **Mg(2) site** | | | |
| Mg (2) Neighbor | Distance (Å) | Mg (2) Neighbor | Distance (Å) |
| N | 1.98 | N | 2.00 |
| H | 2.75 | H | 2.69 |
| Mg | 2.85 | Mg | 2.86 |
| C | 2.97 | H | 2.98 |
| | | C | 2.99 |

**Table S19** Closest neighbors around the calcium (within a 3.0 Å radius) in the organomagnesium structure CCDC 175074.

| **H-optimization** | | **Full optimization** | |
|---|---|---|---|
| Mg Neighbor | Distance (Å) | Mg Neighbor | Distance (Å) |
| N | 1.98 | N | 2.00 |
| N | 1.99 | N | 2.00 |
| O | 2.53 | O | 2.07 |
| H | 2.56 | C | 2.81 |
| C | 2.65 | H | 2.84 |
| H | 2.79 | H | 2.87 |
| H | 2.89 | C | 2.91 |
| H | 2.94 | H | 2.91 |
| C | 2.95 | H | 2.98 |
| H | 2.98 | | |

**Table S20** Closest neighbors around the calcium (within a 3.0 Å radius) in the organomagnesium structure CCDC 266470.

| **H-optimization** | | **Full optimization** | |
|---|---|---|---|
| Mg Neighbor | Distance (Å) | Mg Neighbor | Distance (Å) |
| N | 1.99 | N | 2.00 |
| N | 1.99 | N | 2.00 |
| N | 2.13 | N | 2.15 |
| H | 2.73 | H | 2.75 |
| H | 2.73 | H | 2.75 |
| H | 2.93 | H | 2.99 |
| H | 2.93 | H | 2.99 |
| C | 2.97 | | |
| C | 2.97 | | |

**Table S21** Closest neighbors around the magnesium (within a 3.0 Å radius) in the organomagnesium structure CCDC 266468.

| **H optimization** | | **Full optimization** | |
|---|---|---|---|
| Neighbor | Dist. (Å) | Neighbor | Dist. (Å) |
| N | 1.97 | N | 1.99 |
| N | 2.10 | N | 2.11 |
| N | 2.13 | N | 2.15 |
| H | 2.41 | H | 2.43 |
| H | 2.46 | H | 2.46 |
| H | 2.56 | H | 2.57 |
| H | 2.73 | H | 2.75 |
| H | 2.78 | C | 2.82 |
| C | 2.80 | H | 2.82 |
| C | 2.85 | C | 2.88 |
| C | 2.86 | C | 2.88 |
| Mg | 2.94 | Mg | 2.96 |
| C | 2.96 | C | 2.98 |
| C | 2.99 | | |

**Table S22** Closest neighbors around the magnesium (within a 3.0 Å radius) in the organomagnesium structure CCDC 745088.

| **H optimization** | | **Full optimization** | |
|---|---|---|---|
| Neighbor | Dist. (Å) | Neighbor | Dist. (Å) |
| N | 2.04 | N | 2.05 |
| N | 2.04 | N | 2.06 |
| Mg | 2.81 | Mg | 2.80 |
| C | 2.96 | C | 2.95 |
| C | 2.96 | C | 2.96 |

**Table S23** Closest neighbors around the magnesium (within a 3.0 Å radius) in the organomagnesium structure CCDC 661565.

| | **H optimization** | **Full optimization** |
|---|---|---|
| Mg Neighbor | Distance (Å) | Distance (Å) |
| N | 2.07 | 2.09 |
| N | 2.07 | 2.09 |
| C | 2.49 | 2.50 |
| H | 2.73 | 2.75 |
| H | 2.73 | 2.75 |
| Mg | 2.85 | 2.85 |

**Table S24** Closest neighbors around the magnesium (within a 3.0 Å radius) in the organomagnesium structures CCDC 247151 and 266465.

| | **CCDC 247151** | | **CCDC 266465** | |
|---|---|---|---|---|
| | **H optimization** | **Full optimization** | **H optimization** | **Full optimization** |
| Mg Neighbor | Distance (Å) | Distance (Å) | Distance (Å) | Distance (Å) |
| N | 2.02 | 2.04 | 2.02 | 2.04 |
| N | 2.03 | 2.05 | 2.03 | 2.05 |
| O | 2.05 | 2.09 | 2.05 | 2.09 |
| O | 2.06 | 2.10 | 2.06 | 2.10 |
| C | 2.90 | 2.92 | 2.90 | 2.92 |
| C | 2.91 | 2.93 | 2.91 | 2.94 |

**Table S25** Closest neighbors around the calcium (within a 3.0 Å radius) in the organomagnesium structure CCDC 266466.

| **H-optimization** | | **Full optimization** | |
|---|---|---|---|
| **Mg(1) site** | | | |
| Mg(1) Neighbor | Distance (Å) | Mg (1) Neighbor | Distance (Å) |
| N | 2.03 | N | 2.05 |
| N | 2.03 | N | 2.05 |
| N | 2.17 | N | 2.18 |
| N | 2.19 | N | 2.22 |
| H | 2.83 | H | 2.83 |
| C | 2.91 | C | 2.93 |
| C | 2.93 | C | 2.95 |
| H | 2.94 | H | 2.98 |
| | | | |
| **Mg(1') site** | | | |
| Mg (1') Neighbor | Distance (Å) | Mg (1') Neighbor | Distance (Å) |
| N | 2.03 | N | 2.05 |
| N | 2.03 | N | 2.05 |
| N | 2.16 | N | 2.18 |
| N | 2.18 | N | 2.20 |
| H | 2.94 | C | 2.95 |
| C | 2.96 | C | 2.98 |
| C | 2.97 | H | 2.99 |

**Table S26** Closest neighbors around the magnesium (within a 3.0 Å radius) in the organomagnesium structure CCDC 266464.

| | **H optimization** | **Full optimization** |
|---|---|---|
| Mg Neighbor | Distance (Å) | Distance (Å) |
| N | 2.01 | 2.03 |
| N | 2.01 | 2.03 |
| N | 2.14 | 2.17 |
| N | 2.14 | 2.17 |
| H | 2.97 | |
| H | 2.97 | |

### S7. Simulation of $^{25}$Mg NMR spectra based on the GIPAW calculated NMR parameters

**Table S27** Calculated $^{25}$Mg NMR parameters after H-optimization of structures CCDC 198354, 1477718, 266470, 266465 and 266464.

| | **198354** | | **1477718** | | **266470** | **266465** | **266464** |
|---|---|---|---|---|---|---|---|
| | **Mg(1)** | **Mg(2)** | **Mg(1)** | **Mg(2)** | **Mg** | **Mg** | **Mg** |
| $\delta_{iso}$ (ppm) | 46.3 | 49.0 | 53.5 | 62.1 | 54.7 | 34.8 | 54.1 |
| $\|C_Q\|$ (MHz) | 44.8 | 45.7 | 31.0 | 32.0 | 27.3 | 16.8 | 13.9 |
| $\eta_Q$ | 0.2 | 0.2 | 0.2 | 0.1 | 1.0 | 0.3 | 0.5 |
| $\Omega$ (ppm) | 234.8 | 241.7 | 233.5 | 241.9 | 153.3 | 86.1 | 82.9 |
| $\kappa$ | 0.7 | 0.6 | 0.8 | 0.9 | 0.6 | 0.8 | 0.4 |
| $\alpha$ | 80 | 70 | 125 | 80 | -90 | 80 | 90 |
| $\beta$ | 0 | 0 | 5 | 5 | 90 | 180 | 0 |
| $\gamma$ | −175 | −155 | 10 | 140 | 180 | -20 | 0 |

The relative orientation between the two tensors using three Euler angles ($\alpha$,$\beta$,$\gamma$) was extracted from the first-principles calculations which allows the calculation of the static spectra taking all these parameters into account. The QUEST software was used to simulate spectra (Figure S6). The Euler angles reported therefore describe the relative orientation of the EFG tensor with respect to the shielding tensor along the following conventions: $\delta_{11} \geq \delta_{22} \geq \delta_{33}$ and $|V_{33}| \geq |V_{22}| \geq |V_{11}|$). Span $\Omega = \delta_{11} - \delta_{33}$ and skew $\kappa = 3(\delta_{22} - \delta_{iso})/ \Omega$.

**Figure S6** Simulation of the static $^{25}$Mg NMR spectra at 20 T, for structures CCDC 198354, 1477718, 266470, 266465, 266464, using the QUEST program. Simulations are performed considering a) both the EFG and shielding tensors, or b) only the EFG tensor, showing that for these compounds, the lineshape is dominated by quadrupolar effects. The values calculated in Tables 3-5 for the H-relaxed structures were used in both cases. Euler angles are given in Table S27 (above), while the relative orientation of the shielding and quadrupolar tensors is shown in Figure 4.